Statistical identification of solar wind origins of magnetic impulse events

Ryuho Kataoka and Hiroshi Fukunishi
Department of Geophysics, Tohoku University, Sendai, Miyagi, Japan

Louis J. Lanzerotti[1]
Bell Laboratories, Lucent Technologies, Murray Hill, New Jersey, USA

Received 21 August 2003; revised 24 September 2003; accepted 6 October 2003; published 12 December 2003.

[1] We have compiled a complete list of magnetic impulse events (MIEs) during the 8-year period of 1995–2002 covering solar minimum to solar maximum using fluxgate magnetometer data obtained at the South Pole. Wavelet analysis enables us to detect 825 distinct MIEs automatically with high confidence. Interplanetary magnetic field (IMF) discontinuities are also detected automatically for the same period from Wind and ACE satellite data. From an examination and comparison of the two lists, we find that monthly and seasonal variations in IMF discontinuity occurrences have a significant correlation (0.4–0.5) with those of MIEs. We also find that MIEs tend to occur during intervals of low density, high-speed solar wind streams, and/or radial IMF. No preferences for MIE occurrences are found for solar wind pressure jumps or IMF Bz southward turnings. From detailed minimum variance analysis of 36 IMF discontinuities with one-to-one correspondence to MIEs, ~70% of the IMF discontinuities are found to be tangential discontinuities. The hot flow anomaly (HFA) mechanism can explain at most ~50% of the MIEs; bursty reconnection and pressure pulses can explain the production of at most ~30% and ~20% of the MIEs, respectively. All of the observations and associations are consistent with HFAs or foreshock cavities being the main cause of MIEs. *INDEX TERMS:* 2784 Magnetospheric Physics: Solar wind/magnetosphere interactions; 2109 Interplanetary Physics: Discontinuities; 2134 Interplanetary Physics: Interplanetary magnetic fields; 2724 Magnetospheric Physics: Magnetopause, cusp, and boundary layers; *KEYWORDS:* dayside magnetosphere, solar wind discontinuities, continuous wavelet transform, traveling convection vortices

Citation: Kataoka, R., H. Fukunishi, and L. J. Lanzerotti, Statistical identification of solar wind origins of magnetic impulse events, *J. Geophys. Res.*, *108*(A12), 1436, doi:10.1029/2003JA010202, 2003.

1. Introduction

[2] Magnetic impulse events (MIEs) are identified as impulsive geomagnetic signals measured by ground-based magnetometers with durations of 5–15 min and amplitudes of 50–200 nT occurring in the vicinity of the dayside cusp/cleft latitudes [see *Lanzerotti et al.*, 1991]. Because of their solitary characteristics, MIEs have provided critical clues for understanding some transient responses of the coupled magnetosphere-ionosphere system to solar wind disturbances. MIEs can be characterized as pairs of Hall current loops above ground-based magnetometers [*Lanzerotti et al.*, 1986; *McHenry and Clauer*, 1987]. This idea was introduced as traveling convection vortices (TCVs) [*Friis-Christensen et al.*, 1988; *Glassmeier et al.*, 1989]. In the TCV current system, field-aligned currents connect the ionospheric load with the generator in the dayside magnetosphere.

[3] Various types of transient responses of the magnetosphere work as generators to produce pairs of field-aligned currents. In contrast to sudden commencements (SCs) that are produced by abrupt enhancements of solar wind dynamic pressure [*Araki*, 1994], there is no consensus on the origin of MIEs among researchers. For example, sources of MIEs have been attributed to bursty reconnections [*Lanzerotti et al.*, 1986], solar wind pressure pulses [*Sibeck et al.*, 1989], plasma injections into the low-latitude boundary layer [*Heikkila et al.*, 1989], and Kelvin-Helmholtz instability [*McHenry et al.*, 1990a, 1990b]. Indeed, it is likely that multiple generation mechanisms exist to produce MIEs.

[4] Recently, the bow shock has become considered as a possible source region for MIEs since a hot flow anomaly (HFA), observed in the vicinity of the bow shock, was shown to cause a TCV [*Sitar et al.*, 1998]. Several papers studying the HFA event provided a detailed analysis of the physics behind the bow shock-related interaction [*Sibeck et al.*, 1998, 1999, 2003]. Phenomena similar to HFAs without enhanced temperature and flow deflection are called fore-

[1]Also at Center of Solar-Terrestrial Research, New Jersey Institute of Technology, Newark, New Jersey, USA.

Copyright 2003 by the American Geophysical Union.
0148-0227/03/2003JA010202

shock cavities [*Sibeck et al.*, 2001]. Recently, *Murr and Hughes* [2003], using data from the GEOTAIL satellite just upstream of the bow shock, showed that a vast majority of MIEs in their study resulted from foreshock cavities. In contrast, this paper presents a statistical study of the solar wind origins of MIEs in terms of far upstream solar wind observations.

[5] Both theories and observations have suggested that an important connection exists between solar wind discontinuities and MIEs [*Lanzerotti et al.*, 1987; *Friis-Christensen et al.*, 1988; *Glassmeier et al.*, 1989; *Sibeck et al.*, 1989; *Lin et al.*, 1996; *Cable and Lin*, 1998]. Two types of solar wind discontinuities are frequently observed in the vicinity of the Earth's orbit: tangential discontinuities (TDs) and rotational discontinuities (RDs) [see *Tsurutani and Ho*, 1999, and references therein]. TDs are identified by lack of the magnetic field normal across their surfaces. A TD is considered as a surface separating two different types of plasma because TDs have no mass flux across their surfaces. The magnetic field direction, the magnetic field intensity, plasma densities, plasma temperatures, and even compositions can be different on two sides of a TD surface. TDs are ''frozen in'' to the solar wind and do not propagate with respect to the solar wind. On the other hand, RDs have nonzero normal components of the magnetic field and have mass flow across their surfaces. RDs do not usually have a change in the magnetic field intensity. RDs propagate with respect to the solar wind at the Alfvén speed.

[6] The present study does not rule out RDs despite its relative lack of attention to them because both TDs and RDs could play important roles to produce dayside transients via the bow shock interaction [*Lin et al.*, 1996; *Lin*, 1997]. As a result, we demonstrate statistically herein that the TDs are a more important interplanetary source for producing a MIE transient than are RDs. TDs include abrupt changes in the solar wind dynamic pressure and in the interplanetary magnetic field (IMF), both of which can result in pressure pulses and bursty reconnections. Also, TD-bow shock interactions produce HFAs when the solar wind motional electric field (MEF) points toward the TD [*Schwartz et al.*, 2000].

2. Data Set

2.1. Ground-Based Magnetometers

[7] Data obtained by the fluxgate magnetometer at South Pole (SP) station is used to identify MIEs for the 8-year period of 1995–2002. The magnetic field data used for our analysis consist of three-component vectors with 10-s values in a 24-hour unit, after denoising, interpolating, and resampling with equal time spacing of 10 s. For the same 8-year period, the SYM-H index of the World Data Center for Geomagnetism, Kyoto is also available (available at http://swdcwww.kugi.kyoto-u.ac.jp/). The SYM-H index is essentially the same as Sugiura's hourly Dst index [*Sugiura and Poros*, 1971] except that the SYM-H index consists of 1-min values from a different set of stations and uses a slightly different coordinate system. We used the SYM-H index to identify whether a detected MIE might be the result of a SC or not. Also, careful comparisons between variations in solar wind dynamic pressure and the SYM-H index enable us to adjust and optimize the estimates of the propagation time of interplanetary phenomena measured in space to the ground.

2.2. Solar Wind Monitors

[8] Solar wind data from the Wind and ACE spacecraft have been used in order to provide information on the IMF, solar wind velocity, proton temperature, and proton number density. For convenience, the IMF and other plasma parameters at ACE and Wind that are used in our analysis have been denoised, interpolated, and resampled with an equal time spacing of 64 s using the key parameter data from the CDAWeb (available at http://cdaweb.gsfc.nasa.gov/). In this paper, we require far upstream solar wind data. However, Wind observes bow shock crossings around the time of its perigee. In order to remove from the data set near-Earth data, we used a simple criterion that the satellite location be more than 30 Re upstream. Since the Wind spacecraft moved away from the L1 point after May 1998, we terminated our Wind-based analysis and used ACE data after February 1998. Wind 3-s high-resolution data have been used for detailed classification of IMF discontinuities. OMNI data (available at http://nssdc.gsfc.nasa.gov/omniweb/) of 1-hour averaged solar wind parameters have been used to obtain background solar wind parameters for the 8-year interval studied.

3. Method of Analysis

[9] We made two independent lists of MIEs and IMF discontinuities from the data sets described above. A wavelet analysis was used to detect a large number of distinct MIEs with high confidence as shown in section 3.1. IMF discontinuities were also detected for the same period as shown in section 3.2.

3.1. Magnetometer Data Analysis

[10] Many past statistical studies of MIEs have used visual detection for their event selections [*Glassmeier et al.*, 1989; *Vorobjev et al.*, 1994; *Sibeck and Korotova*, 1996; *Sitar and Clauer*, 1999]. Instead, we used the continuous wavelet transform [*Torrence and Compo*, 1998]. Assume that one has a wavelet function, $\psi_0(\eta)$, that depends on a nondimensional time parameter η. The best wavelet function, especially suitable for objective and reproducible detection of solitary waveforms and therefore to detect MIEs, is the Paul wavelet that has an identical waveform to that of typical MIEs:

$$\psi_0(\eta) = \frac{2^m i^m m!}{\sqrt{\pi(2m)!}}(1 - i\eta)^{-(m+1)}, \tag{1}$$

where m is the order, here taken to be 4. The wavelet function is shown in Figure 1. Assume that one has a time series, x_n, with an equal time spacing δt and $n = 0 \ldots N - 1$. The continuous wavelet transform of a discrete sequence x_n is defined as the convolution of x_n with a scaled and translated version of $\psi_0(\eta)$:

$$W_n(s) = \sum_{n'=0}^{N-1} x_{n'} \psi^* \left[\frac{(n' - n)\delta t}{s} \right], \tag{2}$$

where the (*) indicates the complex conjugate.

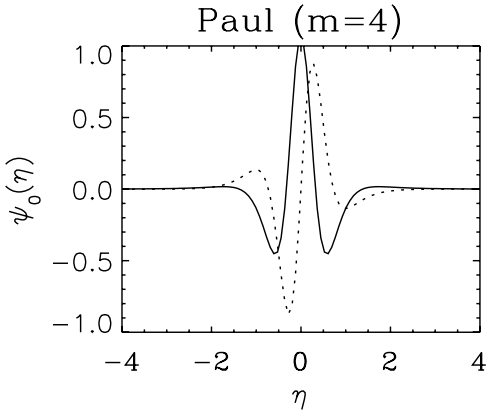

Figure 1. Waveform of the wavelet function used in this paper. The real part and imaginary part for the Paul wavelet in the time domain are plotted by solid and dotted lines, respectively.

[11] For MIE detection, we used the 10-s values of the magnetometer data in each of the three Cartesian geomagnetic coordinate components during an entire day. That is N = 8640 points and δt = 10 s. Here, we define "MIE power" as a scale-averaged wavelet power from 240 s to 640 s normalized by the scale-integrated time-averaged wavelet power with a 90-min running window. For the Paul wavelet with the order of 4, the relationship between the Fourier period λ and the wavelet scale s is $\lambda \sim 1.4s$. In this case, the range of the Fourier period becomes 5.6 min to 14.9 min, corresponding to the normal MIE duration. We selected events in which MIE power is greater than 2. This criterion means that an impulsive target has more than twice the power of the running variance in a 90 min window. This factor of 2 is decided by tuning to find the traditional MIEs in the literature. Note that this criterion is a pattern matching process in any amplitude range and independent of the absolute MIE amplitude itself.

[12] A typical example of our event detection is shown in Figure 2. As alluded to in section 1, MIEs are strongly concentrated on the dayside of the Earth [e.g., *Lanzerotti et al.*, 1991]. Therefore in order to avoid any undesirable effects of the cone of influence [*Torrence and Compo*, 1998] or nighttime substorms, we selected only dayside events occurring between 0600 and 1800 MLT (0930–2130 UT at SP). We defined "MIE timing" as the extremal time of MIE power fulfilling the criteria described above, and the "MIE interval" as 10 min before and after the MIE timing. If MIE timings in different components were within

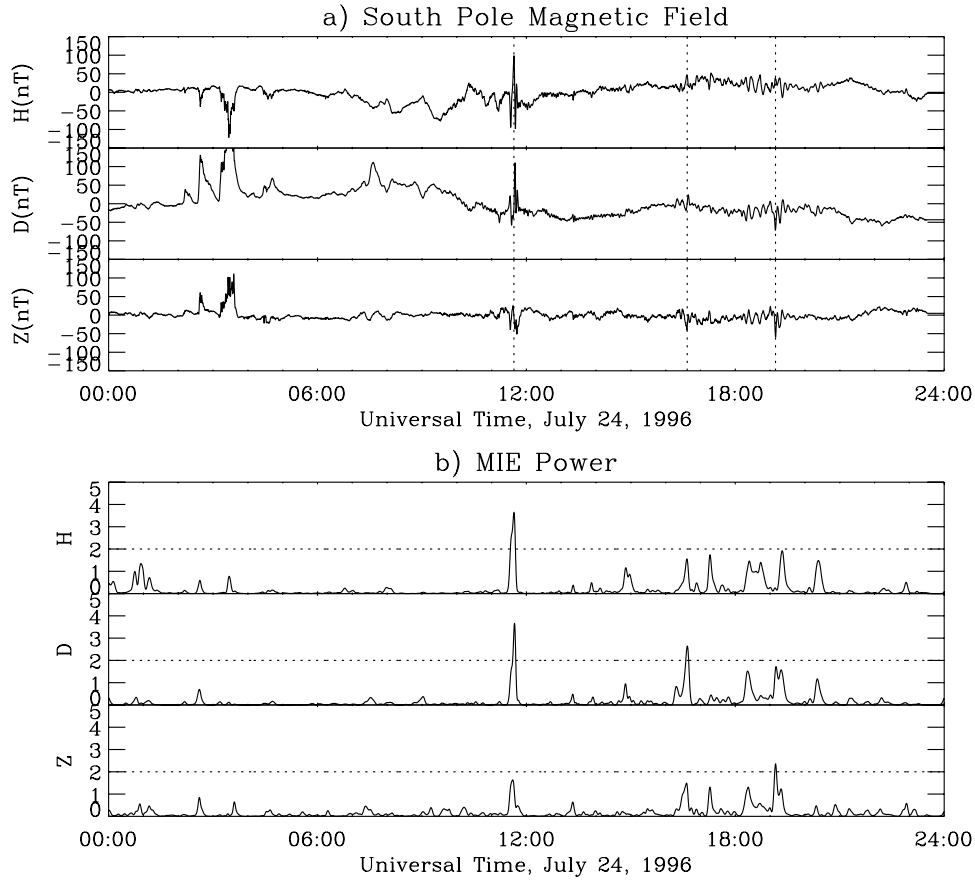

Figure 2. An example of MIE detection on 24 July 1996. The top three panels show the three components of magnetic field for a 24-hour interval measured by the fluxgate magnetometer at South Pole station. The bottom three panels show MIE power for each of three components (see text for the definition). The timings where MIE power is greater than 2 are indicated by vertical dotted lines.

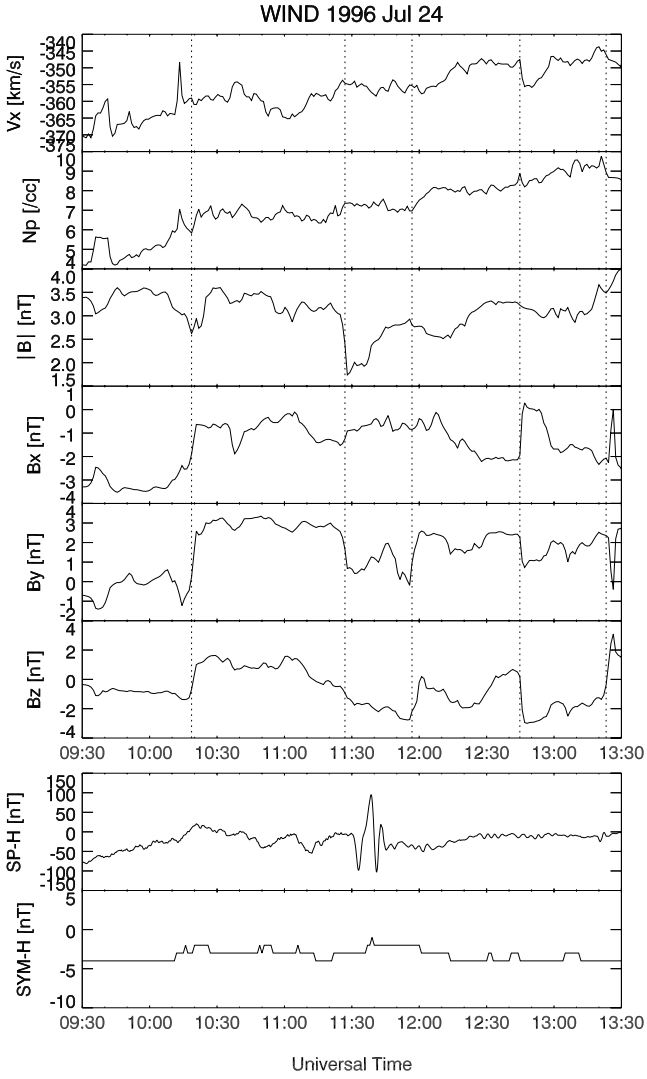

Figure 3. An example of IMF discontinuity detection. From top to bottom, solar wind velocity, proton number density, total IMF, Bx, By, and Bz components in GSM coordinates are shown with the 4-hour interval including a MIE at 1130 UT on 24 July 1996. Detected IMF discontinuities are indicated by vertical dotted lines. The bottom two plots show variations of the H component at South Pole and the SYM-H index.

15 min, we treated these as the same event. Finally, we required that the peak-to-peak amplitude variation be greater than 100 nT during the MIE interval in at least one component.

[13] The wavelet detection described above is tuned to give almost identical detection efficiency in comparison with the studies that have used human eyes of magnetometer specialists. Consequently, the results in this paper are remarkably consistent with previous results in the literature. Our list consists of 825 MIEs over the 8 years and includes "typical" MIEs analyzed in past papers such as 24 January 1996 [*Clauer and Petrov*, 2002], 22 May 1996 [*Kataoka et al.*, 2002, 2003], 24 July 1996 [*Sitar et al.*, 1998; *Sibeck et al.*, 1999; *Kataoka et al.*, 2003], 6 June 1997 [*Kataoka et al.*, 2001], and 27 May1998 [*Kataoka et al.*, 2002]. Also, 8 of 32 events analyzed by *Murr and Hughes* [2003] are included in our list. *Murr and Hughes* [2003] used criteria combining several magnetometers in the Northern Hemisphere to confirm the traveling nature of TCVs. Essentially, our list is almost identical with theirs, with the difference mainly due to the difference of local time coverage between their magnetometer network and South Pole Station.

[14] Various selection criteria of MIEs and TCVs were reviewed by *Zesta et al.* [2002] in detail. The technique used in this study selects "isolated events" in a relatively quiet and magnetically undisturbed background with amplitude significantly larger than any surrounding variations. It is also worthwhile to note that *Zesta et al.* [2002] found many general similarities, but also some differences, between isolated and nonisolated events in their statistical study.

3.2. Solar Wind Data Analysis

[15] Figure 3 shows an example of the 4-hour interval including the MIE detection at the center of the interval near 1130 UT. The timing of the IMF discontinuity is detected using a criterion that the IMF changes its direction by at least 30° within 128 s (using the 64 s resampled data). Multiple discontinuities within 5 min are regarded as a single discontinuity. Detected IMF discontinuities are shown with vertical dotted lines in Figure 3. Our list includes about 4.7×10^4 and 9.7×10^4 IMF discontinuities during the period of 1995–1997 and 1998–2002 for the Wind and the ACE observations, respectively.

[16] The selection of TDs from the detected IMF discontinuities is a central objective of this paper. TDs play the role of a boundary separating different plasma regions. Significant jumps in any of the total magnetic field, ion temperature, or ion number density are the first clue for a TD. On the other hand, the first clue for RDs is a negligible jump in every scalar parameter because RDs do not usually have such magnitude changes, unless there is a significant thermal anisotropy in the transition region [*Hudson*, 1970]. Conventionally, the normal vector of the IMF discontinuity plane is another clue to distinguish TDs and RDs because TDs have no magnetic field across the discontinuity plane, whereas RDs often have.

[17] A minimum variance analysis (MVA) is applied to IMF discontinuities to provide the normal vector **n** of the discontinuity plane by computing the minimum value of the standard deviation, σ, of the magnetic field component in that direction [*Sonnerup and Cahill*, 1967]

$$\sigma^2 = \frac{1}{K}\sum_{k=1}^{K}[\mathbf{B}_k \cdot \mathbf{n} - \langle \mathbf{B} \rangle \cdot \mathbf{n}]^2, \quad (3)$$

where $\mathbf{B}_k$ is the k-th vector field measurement and $\langle \mathbf{B} \rangle$ is the average vector. Minimizing the value of the standard deviation is equivalent to finding the smallest eigenvalue, λ_{min}, of the covariant matrix, although one derives three eigenvalues (λ_{min}, λ_{int}, λ_{max}) from equation (3) where $\lambda_{min} < \lambda_{int} < \lambda_{max}$. We use a 30–120 s interval for MVA using Wind 3-s IMF data and take a cutoff ratio of the intermediate to the minimum eigenvalues $\lambda_{int}/\lambda_{min} > 2$ to define the discontinuities. The time lag between each MIE and corresponding IMF discontinuity is confirmed to be consistent in terms of the derived normal vector **n**. Assuming propagation of the tilted plane of the disconti-

Table 1. Classification Criteria of TD and RD

	Classification Criteria
TD	$\theta < 15^\circ$ and (dn/n > 10%, dV/V > 10%, or dB/B > 20%)
RD	$\theta > 15^\circ$ and (dn/n < 10%, dV/V < 10%, and dB/B < 20%)
Neither	$\theta < 15^\circ$ and (dn/n > 10%, dV/V > 10%, or dB/B > 20%)

nuity, the time lag τ from a satellite location **S** to a given location **P** is given as

$$\tau = \frac{(\mathbf{P} - \mathbf{S}) \cdot \mathbf{n}}{\mathbf{V} \cdot \mathbf{n}}, \tag{4}$$

where **V** is the propagation velocity of the discontinuity. We used a nominal magnetopause at GSE (x, y, z) = (10, 0, 0) as the target and the measured solar wind velocity as **V**. A maximum 20-min error is allowed for this lag coincidence test.

[18] We find 36 MIEs appropriate for the detailed discontinuity analysis. Each of these MIEs has a one-to-one correspondence with an IMF discontinuity. The number of events (36) is low because this one-to-one criterion is quite strict. Under our selection criteria of IMF discontinuities, there are two or more IMF discontinuities that could be the solar wind origin of most of the MIEs. In other words, several IMF discontinuities usually exist in a 1-hour interval around MIE timings.

[19] Since there is no magnetic field across TDs, the normal vector of the TD, $\mathbf{n}_{TD}$, is deduced by a cross product of magnetic fields immediately upstream and downstream of the TD. We define θ as the acute angle between $\mathbf{n}_{TD}$ and **n**. We use parameters θ, dB/B, dn/n, and dV/V to determine whether each event is a RD or a TD with the identification criteria listed in Table 1. Typical examples for TD and RD are shown in Figures 4a and 4b, respectively. The estimated time lag

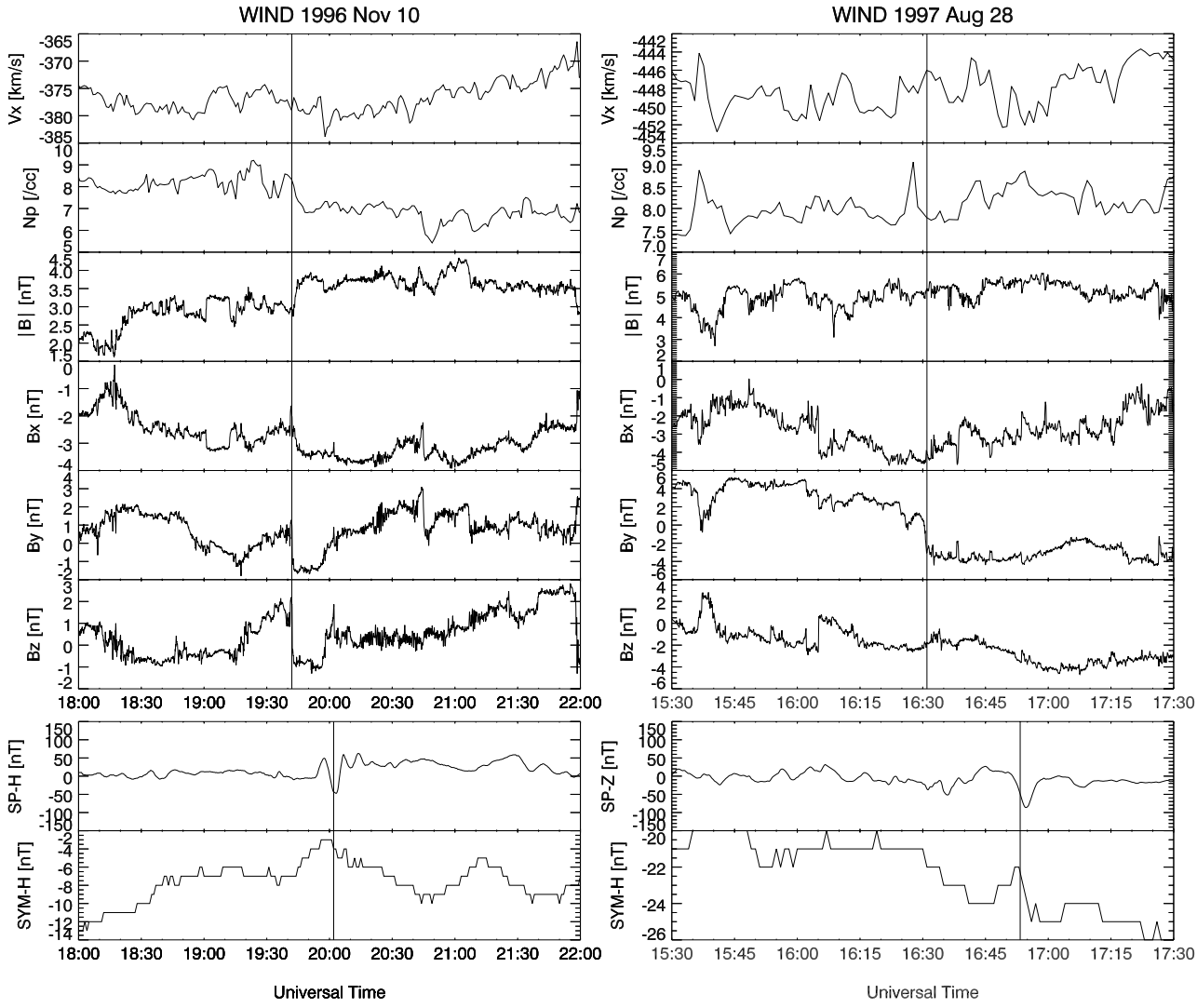

Figure 4. Typical examples of (a) a tangential discontinuity at 1942 UT on 10 November 1996 and (b) a rotational discontinuity at 1631 UT on 28 August 1997. The format is the same as Figure 3 except for using 3-s Wind IMF data. Vertical solid lines in the top panels show the timings of the discontinuities, while those in the bottom panels show the timings of MIEs.

Table 2. MIEs and TDs With One-to-One Correspondence

Number	yymmdd	MIE	TD
1	950205	1603	1452
2	950228	1430	1349
3	950426	1118	0948
4	950826	1358	1341[a]
5	950829	1615	1551
6	950830	1421	1401
7	950913	1349	1400
8	951123	1137	1105
9	960427	1411	1345
10	960522	1311	1256[b]
11	960724	1138	1019[c]
12	960908	1349	1335
13	961002	1250	1236
14	961021	1056	1026
15	961110	2002	1942
16	961210	1528	1518
17	970502	1706	1633
18	970718	1531	1505
19	970724	1338	1315
20	970811	1408	1345
21	970814	1148	1124
22	970820	0956	0915
23	970925	1331	1306
24	970925	1947	1951
25	971003	1417	1402

[a] *Murr and Hughes* [2003].
[b] *Kataoka et al.* [2002].
[c] *Sibeck et al.* [1999].

using equation (4) is 13 min for the 10 November event in Figure 4a, and the observed time lag is 26 min. This is a typical TD event because $\theta = 9°$ and there are significant jumps in n and B. The estimated time lag using equation (4) is 23 min for the 28 August event in Figure 4b, and the observed time lag is 21 min. This is a typical RD event because $\theta = 90°$ and there are negligible jumps in n, V, and B. The 25 TD events and the remaining 11 events are listed in Tables 2 and 3.

4. Results

[20] Statistical results for the occurrences of the 825 MIEs are shown in Figure 5. The MIEs in Figure 5 are divided into two types in terms of the amplitudes of the SYM-H fluctuations: noncompressive MIEs with <5 nT SYM-H perturbations (solid histograms) and compressive MIEs with >5 nT SYM-H perturbations (lighter histograms). From Figure 5a, we can find that MIEs with significant global compression/expansion are about 17%. Also, a number of SCs are actually included in the 825 events. When we define the SCs as the events with >10 nT step-like jump within 10 min in the SYM-H index, a total of 66 SCs are found in the 825 events. This accounts for 8.0% of 825 MIEs.

[21] Figure 5b shows the long-term trend of the annual number of MIEs in the period 1995–2002. The occurrence of compressive MIEs increases from solar minimum to solar maximum. This suggests that the solar wind driver of MIEs tends to be more compressive in the maximum phase. Figure 5c shows MIE occurrences versus MLT for the 8-year period 1995–2002. The double-peak distribution around local noon originally reported by *Lanzerotti et al.* [1991] is reproduced. The double-peak distribution is supported by only one local time histogram value, a large dip in occurrence in the 1200 MLT bin. All other histogram values would be consistent with a broad, single-peak distribution. The distribution in Figure 5c shows that the occurrence maximizes in local morning hours, consistent with many other studies [*Glassmeier et al.*, 1989; *Vorobjev et al.*, 1999; *Zesta et al.*, 2002]. Figure 5d shows a scatter plot of the peak-to-peak amplitudes of MIEs versus MLT. Only the noncompressive events (total of 687 events) are plotted. The maximum amplitude tends to be larger in the prenoon sector and smaller in the postnoon sector. A similar distribution was reported by *Sibeck and Korotova* [1996].

[22] Now we turn to a comparison of the lists of the 825 MIEs and the 14.4×10^4 IMF discontinuities. Figure 6 shows the variations in the occurrences of the MIEs and IMF discontinuities as histograms in 14-day intervals for each of the 8 years separately. Both histograms show similar trends over monthly and seasonal time-scales. The correlation coefficients between the number of MIEs and that of IMF discontinuities are 0.48 and 0.40 for 1995–1997 Wind data and 1998–2002 ACE data, respectively. These correlation coefficients are statistically significant and suggest that they are related.

[23] Figure 7 shows the normalized MIE occurrence distributions (825 MIEs) as functions of the IMF orientations in the X-Y plane (top left), the X-Z plane (top right), solar wind velocity (bottom left), and density (bottom right). The shaded areas indicate the occurrences of median values for the intervals of 30 min before and after the 825 MIEs, whereas the areas outlined by the thick solid lines indicate the distributions of the interplanetary parameters for the entire interval 1995–2002 from OMNI 1-hour averaged data. In all cases the solar wind data are shifted in time to the magnetopause position according to the measured solar wind velocity and the separation distance along the Sun-Earth line assuming a flat and nontilted discontinuity plane. The magnetopause is taken

Table 3. MIEs and RDs With One-to-One Correspondence (Left) and Others (Right)

Number	yymmdd	MIE	RD	Number	yymmdd	MIE	Others
1	950228	1456	1408	1	950129	1245	1212
2	950527	1612	1525	2	950604	2044	1946
3	950828	1221	1155	3	951104	1904	1825
4	950828	1813	1749				
5	950828	1836	1805				
6	970504	1141	1046				
7	970801	1057	1035				
8	970828	1653	1631				

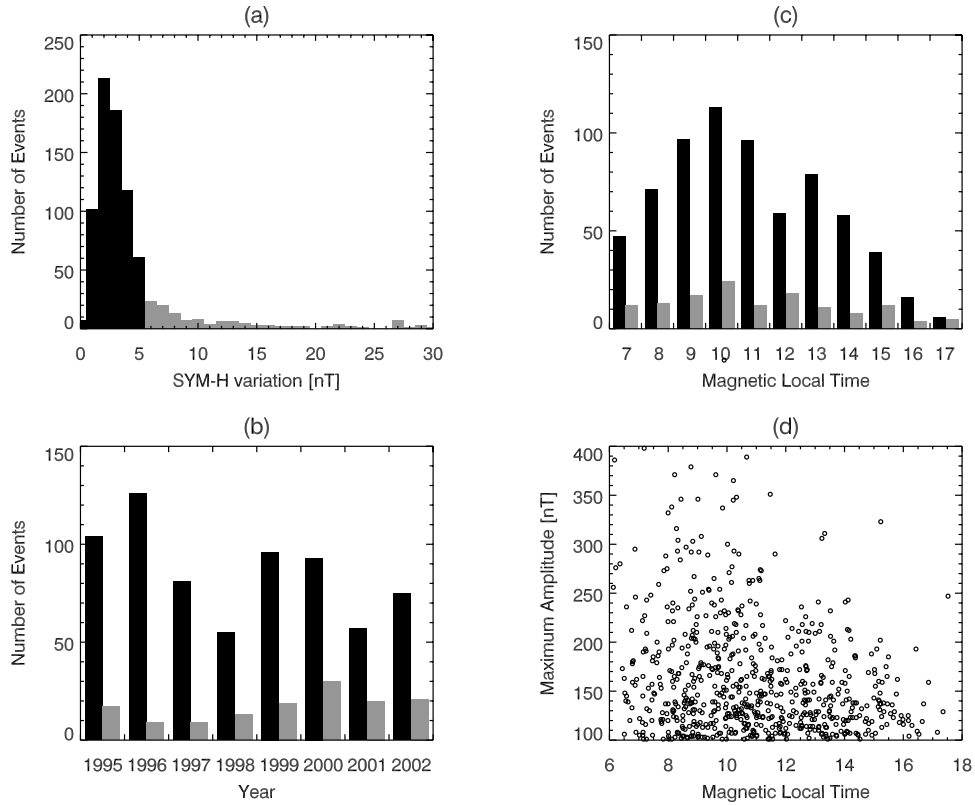

Figure 5. MIE occurrence distributions: (a) histograms of MIE occurrence versus magnitude of SYM-H perturbations, (b) histograms of MIE occurrence versus MLT, (c) long-term variations of the annual number of MIEs from 1995 to 2002, (d) scatter plot of maximum amplitude versus MLT. Gray and black histograms identify the compressive MIEs with >5 nT SYM-H perturbations and noncompressive MIEs with <5 nT SYM-H perturbations, respectively.

as a target at GSE (x, y, z) = (10, 0, 0) for the arrival estimation. As shown in this Figure 7, MIEs basically occur under a wide range of solar wind conditions. A preference for a radial IMF (Figure 7a) is consistent with previous statistical results [*Konik et al.*, 1994; *Sibeck and Korotova*, 1996; *Vorobjev et al.*, 1999]. We also find that MIE occurrence increases in low-density (Figure 7d) and high-speed (Figure 7c) solar wind.

5. Discussion

[24] First, we discuss the cause of the long-term trends in the occurrences of MIEs and of IMF discontinuities. Figure 8a shows these two quantities, averaged over the 8 years 1995–2002. The histograms of MIEs and IMF discontinuities are shown by thick solid line and thin solid line with vertical tick marks, respectively. The occurrences of MIEs are characterized by a weak semiannual variation with maxima in the spring and fall seasons. The occurrences of discontinuities also have a maximum in the fall. The absence of a maximum in the spring is because of the occurrence of large fluctuations in the number of discontinuities in the January to March time interval during the solar maximum that we analyzed. For example, it is clear from Figure 6 that the triple peaks in the beginnings of January, February, and March are found in both 2000 and 2001. A similar semiannual trend of MIE occurrences was reported by *Sibeck and Korotova* [1996], based on magnetometer data acquired in the Northern Hemisphere. In contrast, however, *Glassmeier et al.* [1989] found a minimum in occurrence during equinoxes in their statistical study, and *Zesta et al.* [2002] concluded that there is no clear seasonal variation for TCV events.

[25] It is also worthwhile to note here that there is an apparent preference in MIE occurrences for high-speed and low-density solar wind conditions. These are type of conditions that are associated with coronal hole streams, although the times of MIE occurrences also include many intervals with normal conditions or even conditions opposite to those expected for coronal holes. *Tsurutani and Ho* [1999] have shown that the number of IMF discontinuities increases in solar wind originating from coronal holes. The semiannual variation of MIE occurrence may be explained by the 7° declination of the Sun's rotation axis to the ecliptic plane. In this geometry, high-speed streams from coronal holes with inward (outward) IMF tend to hit the Earth in spring (fall). A similar but more complicated effect has been discussed for geomagnetic activity for a long time [e.g., *Russell and McPherron*, 1973]. Figure 8b shows histograms for the durations of high-speed (>600 km/s) streams, averaged over the 8-year interval of 1995–2002. It is clear that the durations of the streams with inward (outward) IMF increase in spring (fall), consistent with the hypothesis. However, the solar wind condition of high-speed streams

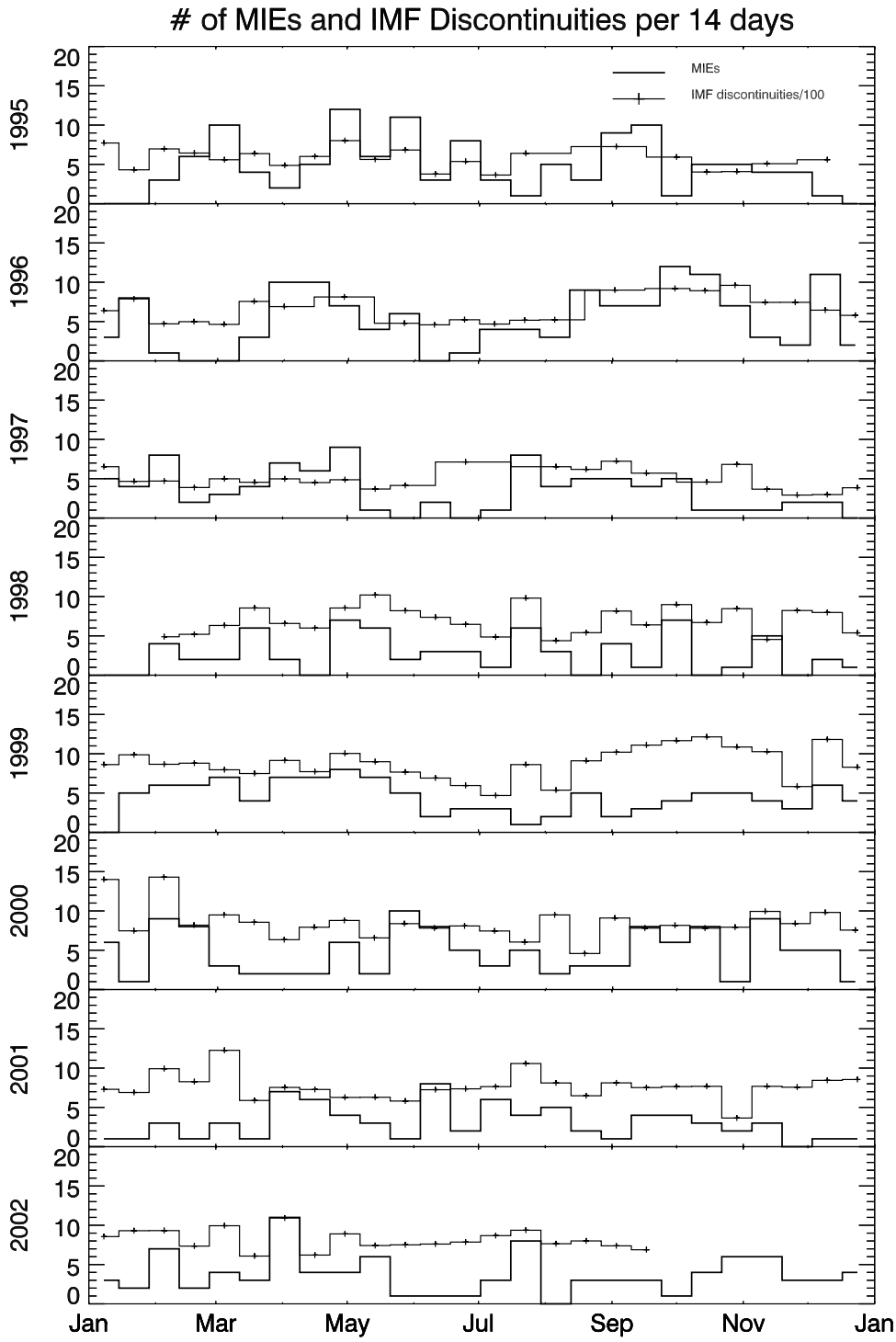

Figure 6. Variations in the numbers of MIEs and IMF discontinuities occurring during each year of the 8-year period of 1995–2002. Each number corresponds to a 14-day interval.

and low densities are inconsistent with previous statistical results concerning the occurrence conditions of MIEs [e.g., *Sibeck and Korotova*, 1996; *Vorobjev et al.*, 1999]. This discrepancy may be due to different data sets. Most significantly, our MIE list has 825 events covering solar minimum to solar maximum conditions. The number of large-amplitude MIEs is the largest studied to date, and the covered time interval is also the longest.

[26] Second, we discuss the solar wind origins and generation mechanisms of MIEs. TDs could include several different mechanisms for producing MIEs as previously proposed, such as bursty reconnection, pressure pulses, and hot flow anomalies [see *Kataoka et al.*, 2002]. It is important to find the contribution rates of the possible individual driving mechanisms for the production of impulsive ground magnetometer deflections.

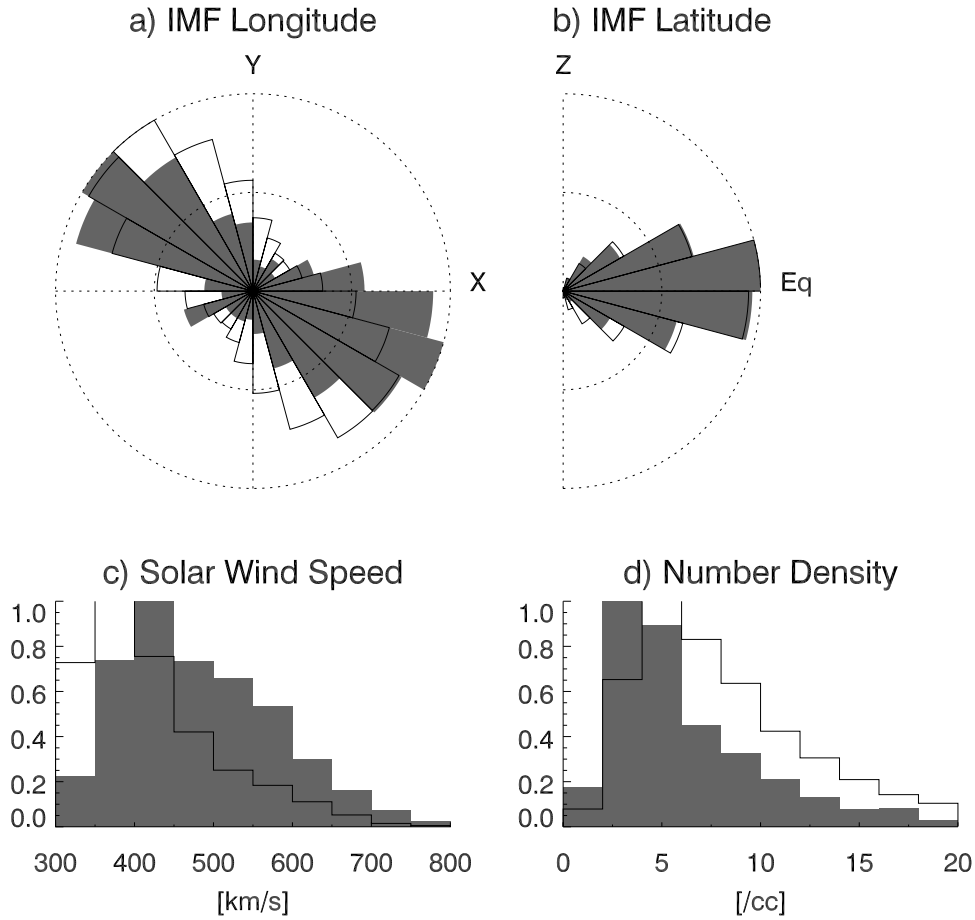

Figure 7. Histograms of the MIE event occurrence versus solar wind parameters. Plotted are normalized occurrences versus (a) longitude and (b) latitude of IMF in GSM coordinates, (c) solar wind velocity, and (d) proton number density. The shaded areas indicate the occurrences in the intervals 30 min before and after the timings of the MIEs, whereas the black lines indicate the distribution for the entire 8-year period using OMNI 1-hour averaged data.

Out of the 36 events listed in Tables 2 and 3, the numbers of positive, negative and no Bz turnings are 11, 12, and 13, respectively. From this result, we can conclude that the bursty reconnection mechanism explains at most ~30% of MIEs. There are six MIEs with SYM-H variations >5 nT in this list. From this result, we conclude that the pressure pulse mechanism explains at most ~20% of MIEs. The small number of events that are related to pressure pulses is consistent with previous studies [*Konik et al.*, 1994; *Sibeck and Korotova*, 1996; *Vorobjev et al.*, 1999]. Note that this occurrence rate of compressive MIEs is very similar to the result of Figure 5a. On the other hand, there are 25 TDs, eight RDs, and three others in Tables 2 and 3. That is, ~70% of the IMF discontinuities that are associated with MIEs are TDs. These TDs have special characteristics as discussed below.

[27] Previous studies have shown that the formation of a HFA requires solar wind motional electric fields (MEF) pointing toward the TD, at least on one side of the TD [*Schwartz*, 2000]. Figure 9 shows a scatter plot of the angles between the 25 TD normal vectors and the MEF (corresponding to the events in Table 2). The five (of 25) TD events (20%) in the right bottom sector do not have inward pointing MEF on either side. It is important to note that these five events are accompanied by positive or negative IMF Bz turnings. Figure 10 shows the directions of the TD normal vectors associated with MIEs in the RTN coordinate system with R radially out from the Sun and N northward. The asterisk indicates the Parker spiral direction (45° toward the right). We classified the TDs into three groups: TDs related to the MIEs occurring in the dawn (dusk) sector are indicated by triangles (crosses). Other events in the noon sector (1100–1300 MLT) are indicated by filled circles. It is found from this result that the orientations of TDs control the generation sites of MIEs. The same TD will first lie tangent to the bow shock on one side, then intersect it on the same side, and then intersect it on the other side. MIEs are more common on the dusk side when TDs intersect the dusk bow shock at a perpendicular angle, and vice-versa. The large cone angle of the TD normal (>~40°) is another condition for enhancement of the TD-bow shock interaction. HFAs prefer such a condition because the effective time of the interaction between the TD and the bow shock becomes longer [*Schwartz*, 2000]. Combining the above two HFA criteria of inward IMF and large cone angle, there are

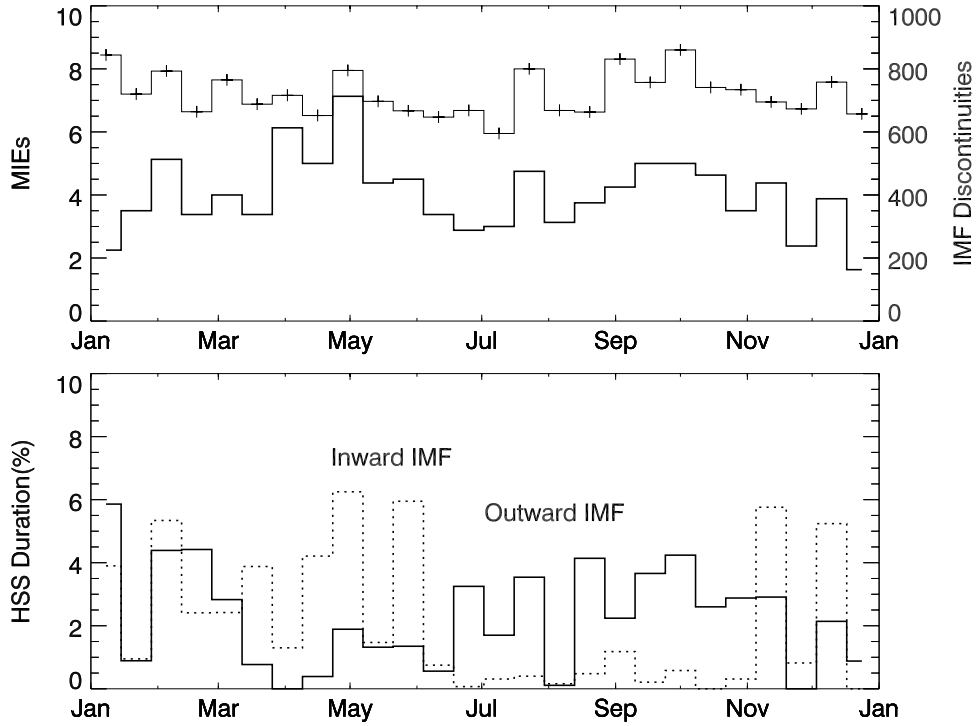

Figure 8. (a) Averaged occurrences of MIEs and TDs integrated over the 8-year period of 1995–2002. The histograms of MIEs and IMF discontinuities are shown by thick solid line and thin solid line with vertical tick marks, respectively. (b) Histograms for the durations of high-speed (>600 km/s) streams averaged over the 8-year interval of 1995–2002. High-speed streams with inward and outward IMF are distinguished as dotted and solid lines, respectively.

17 TD events that satisfy both criteria simultaneously. Since a total 36 MIEs (25 TDs, eight RDs, and three others) were selected, we can conclude that HFAs can explain at most 50% of MIEs.

[28] Finally, we discuss the importance of the interaction between the solar wind and the bow shock. Our results confirm that low density, high-speed solar wind conditions, and/or radial IMF conditions are evidently more favorable for MIEs than are average conditions. We found no preferences for occurrences in pressure jumps or IMF Bz southward turnings. A significant correlation in the occurrences of MIEs and IMF discontinuities was found from the long-term analysis. Furthermore, we found preferences in MIE occurrences for TDs with inward MEF and large cone angles, conditions that are the empirical criteria for HFA formation at the bow shock [*Schwartz*, 2000]. High-speed stream and radial IMF enhance the interaction between the bow shock and incoming solar wind to produce foreshock cavities via the ion beam instability [*Sibeck et al.*, 2001]. The fact that approximately 100 times as many IMF discontinuities as MIEs are observed suggests that IMF discontinuities themselves are an inefficient source of MIEs. Some special properties, such as TDs with inward pointing MEF, should be needed when an IMF discontinuity is a necessary condition for triggering a MIE. Or there could be other driving factors. For example, IMF discontinuities are more common under high-speed stream and so are MIEs, and foreshock cavities are sensitive and unstable to produce MIEs under such conditions. All of the observa-

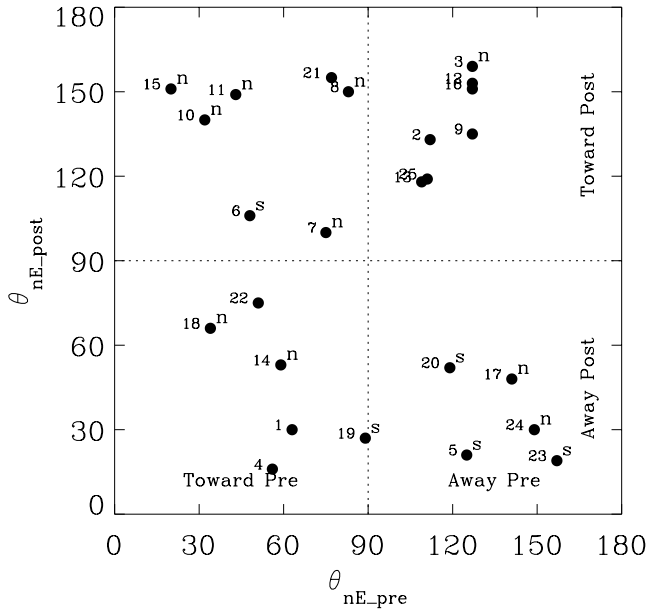

Figure 9. Scatter plot of the angle between the TD normal vector **n** and the solar wind motional electric field **E** = $-\mathbf{V} \times \mathbf{B}$ in the region prior to (horizontal) and after (vertical) TD passage. Events labeled "n" and "s" have northward and southward IMF turnings, respectively. The unlabeled events have no IMF turnings. Event number of Table 2 is indicated for each event. Sectors corresponding to the electric field pointing toward/away from the TD are also labeled.

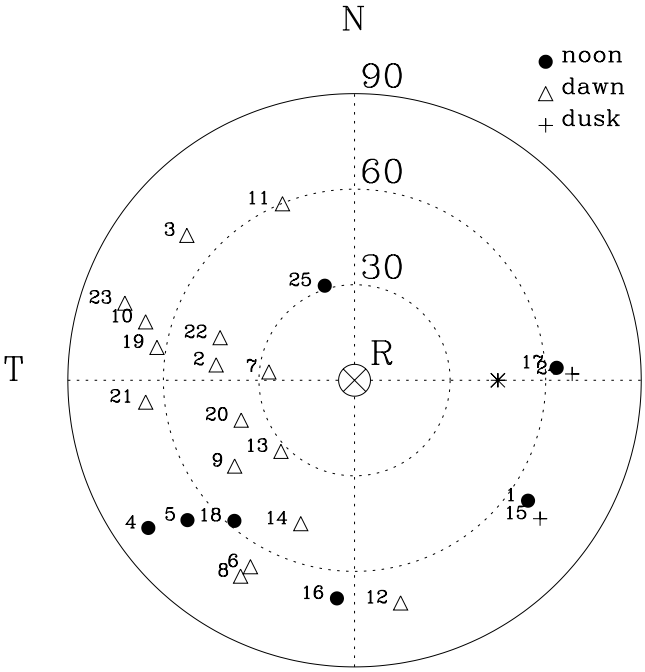

Figure 10. Directions of normal vectors to TDs associated with MIEs. The normal vectors are displayed in the RTN coordinate system, with R radially out from the Sun, N northward, and T completes the right-handed triad. The plot shows the view from the Sun, with T to the left and N toward the top. The radial coordinate in the plot gives the cone angle from the R axis from 0° (center) to 90° (outer edge). Conventionally, normal vectors are reversed as is required to ensure positive R components. Occurrences of MIEs in the dawn (dusk) sector are indicated by triangles (crosses). Other MIEs in the noon sector (1100–1300 MLT) are indicated by solid circles. Event number of Table 2 is indicated for each event. The asterisk indicates the Parker spiral direction (45° toward the right).

tions and associations are consistent with HFAs or foreshock cavities being the main cause of MIEs.

6. Conclusion

[29] Using simple artificial intelligence software, we compiled complete lists of MIEs and IMF discontinuities during an 8-year period (1995–2002) that covers solar minimum to solar maximum. From statistical comparisons between the two lists, we found that monthly and seasonal variations in IMF discontinuity occurrences have a significant correlation with those of MIEs. We also found that MIEs tend to occur during intervals of low density, high-speed solar wind streams, and/or radial IMF. No preferences for the occurrence of MIEs are found for times of solar wind pressure jumps or IMF Bz southward turnings. Of the 36 one-to-one correspondence events between MIEs and IMF discontinuities, ~70% of IMF discontinuities are found to be TDs. The HFA mechanism can explain at least ~50% of the MIEs, with bursty reconnection or pressure pulses possibly associated with about ~30% and ~20% of the MIEs, respectively.

[30] **Acknowledgments.** We thank the NSSDC CDAWeb and OMNIWeb for supplying solar wind data used in this study. Wavelet software was provided by C. Torrence and G. Compo, and is available at URL http://paos.colorado.edu/research/wavelets/. The research at NJIT was supported in part by the United States National Science Foundation Office of Polar Programs through the University of Maryland.

[31] Lou-Chuang Lee thanks David Sibeck and Mark Engebretson for their assistance in evaluating this paper.

References

Araki, T., A physical model of the geomagnetic sudden commencement, in *Solar Wind Sources of Magnetospheric Ultra-Low-Frequency Waves*, *Geophys. Monogr. Ser.*, vol. 81, edited by M. J. Engebretson, K. Takahashi, and M. Scholer, p. 183, AGU, Washington, D. C., 1994.

Cable, S., and Y. Lin, Three-dimensional MHD simulations of interplanetary rotational discontinuities impacting the Earth's bow shock and magnetosheath, *J. Geophys. Res.*, *103*, 29,511, 1998.

Clauer, C. R., and V. G. Petrov, A statistical investigation of traveling convection vortices observed by the west coast Greenland magnetometer chain, *J. Geophys. Res.*, *107*(A7), 1148, doi:10.1029/2001JA000228, 2002.

Friis-Christensen, E., M. A. McHenry, C. R. Clauer, and S. Vennerstrom, Ionospheric traveling convection vortices observed near the polar cleft: A triggered response to sudden changes in the solar wind, *Geophys. Res. Lett.*, *15*, 253, 1988.

Glassmeier, K.-H., M. Honisch, and J. Untiedt, Ground-based and satellite observations of traveling magnetospheric convection twin vortices, *J. Geophys. Res.*, *94*, 2520, 1989.

Heikkila, W., T. Stockflet-Jorgensen, L. J. Lanzerotti, and C. G. Maclennan, A transient auroral event on the dayside, *J. Geophys. Res.*, *94*, 15,291, 1989.

Hudson, P. D., Discontinuities in an anisotropic plasma and their identification in the solar wind, *Planet. Space Sci.*, *18*, 1611, 1970.

Kataoka, R., H. Fukunishi, L. J. Lanzerotti, C. G. Maclennan, H. U. Frey, S. B. Mende, J. H. Doolittle, T. J. Rosenberg, and A. T. Weatherwax, Magnetic Impulse Event: A detailed case study of extended ground and space observations, *J. Geophys. Res.*, *106*, 25,873, 2001.

Kataoka, R., H. Fukunishi, L. J. Lanzerotti, T. J. Rosenberg, A. T. Weatherwax, M. J. Engebretson, and J. Watermann, Traveling convection vortices induced by solar wind tangential discontinuities, *J. Geophys. Res.*, *107*(A12), 1455, doi:10.1029/2002JA009459, 2002.

Kataoka, R., H. Fukunishi, K. Hosokawa, H. Fujiwara, A. S. Yukimatu, N. Sato, and Y.-K. Tung, Transient production of F region irregularities associated with TCV passage, *Ann. Geophys.*, *21*, 1531, 2003.

Konik, R. M., L. J. Lanzerotti, A. Wolfe, C. G. Maclennan, and D. Venkatesan, Cusp latitude magnetic impulse events: 2. Interplanetary magnetic field and solar wind conditions, *J. Geophys. Res.*, *99*, 14,831, 1994.

Lanzerotti, L. J., L. C. Lee, A. Wolfe, C. Maclennan, A. Wolfe, and L. V. Medford, Possible evidence of flux transfer events in the polar ionosphere, *Geophys. Res. Lett.*, *13*, 1089, 1986.

Lanzerotti, L. J., R. D. Hunsucker, D. Rice, L. C. Lee, A. Wolfe, C. G. Maclennan, and L. V. Medford, Ionosphere and ground-based response to field-aligned currents near the magnetospheric cusp regions, *J. Geophys. Res.*, *92*, 7739, 1987.

Lanzerotti, L. J., R. M. Konik, and A. Wolfe, Cusp latitude magnetic impulse events: 1. Occurrence statistics, *J. Geophys. Res.*, *96*, 14,009, 1991.

Lin, Y., Generation of anomalous flows near the bow shock by its interaction with interplanetary discontinuities, *J. Geophys. Res.*, *102*, 24,265, 1997.

Lin, Y., D. W. Swift, and L. C. Lee, Simulation of pressure pulses in the bow shock and magnetosheath driven by variations in interplanetary magnetic field direction, *J. Geophys. Res.*, *101*, 27,251, 1996.

McHenry, M. A., and C. R. Clauer, Modeled ground magnetic signatures of flux transfer events, *J. Geophys. Res.*, *92*, 11,231, 1987.

McHenry, M. A., C. R. Clauer, E. Friis-Christensen, P. T. Newell, and J. D. Kelly, Ground observations of magnetospheric boundary layer phenomena, *J. Geophys. Res.*, *95*, 14,995, 1990a.

McHenry, M. A., C. R. Clauer, and E. Friis-Christensen, Relationship of solar wind parameters to continuous, dayside, high latitude traveling ionospheric convection vortices, *J. Geophys. Res.*, *95*, 15,007, 1990b.

Murr, D. L., and W. J. Hughes, Solar wind drivers of Traveling Convection Vortices, *Geophys. Res. Lett.*, *30*(7), 1354, doi:10.1029/2002GL015498, 2003.

Russell, C. T., and R. L. McPherron, The semiannual variation of geomagnetic activity, *J. Geophys. Res.*, *78*, 92, 1973.

Schwartz, S. J., Conditions for the formation of hot flow anomalies at Earth's bow shock, *J. Geophys. Res.*, *105*, 12,639, 2000.

Sibeck, D. G., and G. I. Korotova, Occurrence patterns for transient magnetic field signatures at high latitudes, *J. Geophys. Res.*, *101*, 13,413, 1996.

Sibeck, D. G., W. Baumjohahnn, and R. E. Lopez, Solar wind dynamic pressure variations and transient magnetospheric signatures, *Geophys. Res. Lett.*, *16*, 13, 1989.

Sibeck, D. G., N. L. Borodkova, G. N. Zastenker, S. S. Romanov, and J.-A. Sauvaud, Gross deformation of the dayside magnetosphere, *Geophys. Res. Lett.*, *25*, 453, 1998.

Sibeck, D. G., et al., Comprehensive study of the magnetospheric response to a hot flow anomaly, *J. Geophys. Res.*, *104*, 4577, 1999.

Sibeck, D. G., R. B. Decker, D. G. Mitchell, A. J. Lazarus, R. P. Lepping, and A. Szabo, Solar wind preconditioning in the flank foreshock: IMP8 observations, *J. Geophys. Res.*, *106*, 21,675, 2001.

Sibeck, D. G., N. B. Trivedi, E. Zesta, R. B. Decker, H. J. Singer, A. Szabo, H. Tachihara, and J. Watermann, Pressure-pulse interaction with the magnetosphere and ionosphere, *J. Geophys. Res.*, *108*(A2), 1095, doi:10.1029/2002JA009675, 2003.

Sitar, R. J., and C. R. Clauer, Ground magnetic response to sudden changes in the interplanetary magnetic field orientation, *J. Geophys. Res.*, *104*, 28,343, 1999.

Sitar, R. J., J. B. Baker, C. R. Clauer, A. J. Ridley, J. A. Cumnock, V. O. Papitashvili, J. Spann, M. J. Brittnacher, and G. K. Parks, Multi-instrument analysis of the ionospheric signatures of a hot flow anomaly occurring on June 24, 1996, *J. Geophys. Res.*, *103*, 23,357, 1998.

Sonnerup, B. U. O., and L. J. Cahill, Magnetopause structure and attitude from Explorer 12 observations, *J. Geophys. Res.*, *72*, 171, 1967.

Sugiura, M., and D. J. Poros, Hourly values of equatorial Dst for years of 1957 to 1970, *Rep. X-645-71-278*, NASA Goddard Space Fight Cent., Greenbelt, Md., 1971.

Torrence, C., and G. P. Compo, A practical guide to wavelet analysis, *Bull. Annu. Meteorol. Soc.*, *79*, 61, 1998.

Tsurutani, B. T., and C. M. Ho, A review of discontinuities and Alfven waves in interplanetary space: Ulysses results, *Rev. Geophys.*, *37*, 517, 1999.

Vorobjev, V. G., V. L. Zverev, and G. V. Starkov, Geomagnetic impulses in the daytime high latitude region: Main morphological characteristics and association with the dynamics of the daytime aurora, *Geomagn. Aeron.*, Engl. Transl., *33*, 621, 1994.

Vorobjev, V. G., O. I. Yagodkina, and V. L. Zverev, Morphological features of bipolar magnetic impulse events and associated interplanetary medium signatures, *J. Geophys. Res.*, *104*, 4595, 1999.

Zesta, E., W. J. Hughes, and M. J. Engebretson, A statistical study of traveling convection vortices using the Magnetometer Array for Cusp and Cleft Studies, *J. Geophys. Res.*, *107*(A10), 1317, doi:10.1029/1999JA000386, 2002.

H. Fukunishi and R. Kataoka, Department of Geophysics, Tohoku University, Sendai, Miyagi 980-8578, Japan. (fuku@pat.geophys.tohoku.ac.jp; ryuho@pat.geophys.tohoku.ac.jp)

L. J. Lanzerotti, Bell Laboratories, Lucent Technologies, Murray Hill, NJ 07974-0636, USA. (ljl@lucent.com)